Supplementary information for "Orientational order of one-patch colloidal particles in two dimensions"

Yasutaka Iwashita, and Yasuyuki Kimura

Department of Physics, Kyushu University, 812-8581 Fukuoka, Japan

CONTENTS

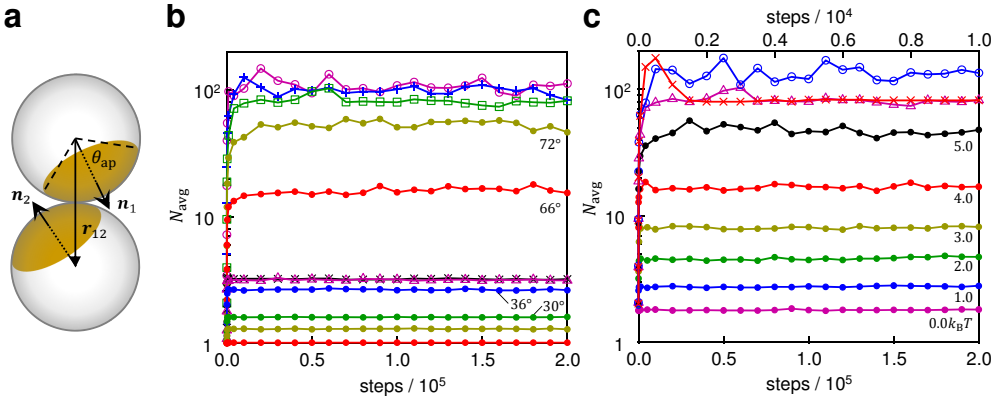

FIG. A A schematic drawing of neighboring one-patch particles in (a) and the development of clustering in the simulation without patch-substrate attraction in (b) and (c). (b): Patch size dependence of the development of N_{avg} plotted against simulation steps. $e_{\mathrm{b}} = 6.0 k_{\mathrm{B}}T$, and θ_{ap} of the plots are 6, 18, 30, 36, 42, 60, 66, 72, 78, 84 and 90° from the bottom, respectively. The symbols of overlapping plots are as follows: (42°, △), (60°, ×), (78°, □), (84°, +), (90°, ○). (c): Inter-patch attraction dependence of the development of N_{avg} for $\theta_{\mathrm{ap}} = 78°$. e_{b} of the plots are 0.0, 1.0, 2.0, 3.0, 4.0, 5.0, 6.0, 7.0 and 10.0 $k_{\mathrm{B}}T$ from the bottom, respectively. The top horizontal axis is for 0.0, 1.0, 2.0, and 3.0 $k_{\mathrm{B}}T$, and the bottom axis is for the others. The symbols of overlapping plots are as follows: ($6.0k_{\mathrm{B}}T$, △), ($7.0k_{\mathrm{B}}T$, ○) and ($10.0k_{\mathrm{B}}T$, ×). In (b) and (c) larger N_{avg} than 80 is predominantly because of the effect of boundary conditions as described in the main text.

SIMULATION METHODS

The pairwise interaction potential between neighboring particle 1 and 2, u_{12}, is written as follows (see Fig. A (a) for the model):

$$u_{12}(\boldsymbol{n}_1, \boldsymbol{n}_2, \boldsymbol{r}_{12}) = \begin{cases} -e_{\mathrm{b}} & \text{if} \quad \boldsymbol{n}_1 \cdot \hat{\boldsymbol{r}}_{12} > \cos\theta_{\mathrm{ap}} \\ & \text{and} \quad \boldsymbol{n}_2 \cdot \hat{\boldsymbol{r}}_{12} < -\cos\theta_{\mathrm{ap}} \\ 0 & \text{otherwise} \end{cases}$$

where $\hat{\boldsymbol{r}}_{12} = \boldsymbol{r}_{12}/r_{12}$, $r_{12} = d$ and $\boldsymbol{r}_{12}$ is the vector from the center of particle 1 to that of particle 2.

In a rectangular simulation box an axis of the triangular lattice of arranged particles is

parallel to y-axis, and 40 particles are arranged in y direction. For x-direction 46 particles are arranged in a zig-zag manner.

In a simulation step, a random three-dimensional rotational move is attempted for each particle. The initial orientations of particles are randomized. For efficient relaxation of clustering the range of rotation is changed in a simulation run: In the first quarter of the total steps the rotation is within $\pm\pi$ rad, in the second $\pm\pi/3$ rad, in the third $\pm\pi/9$ rad and in the last $\pm\pi/30$ rad. The total steps are from 10^4 to 2×10^5 dependent on the parameters. For a set of e_b and θ_ap, four independent simulation runs were carried out. As shown in Fig. A (b) and (c), N_avg reaches its steady value in the very early stage of a simulation run. After the runs, we have never found any other steady cluster states than the ones described in the main text.

ANALYSIS BY IMAGE PROCESSING

Analyses in Section 3.1.1 to 3.1.3

In a linear cluster the patches aggregates around its middle in width, we thus analyze the dark regions in an image. A microscopy image is binarized and skeletonized with a software, ImageJ (see the lines in Fig. B (b)). An obtained line is segmented by equal length measured along the line (see Fig. B (c)), and the average length for segmentation is chosen to 2.34 μm to avoid angular fluctuation by zigzag undulation in a linear cluster. For the mapping of orientation an end-to-end or -node segment shorter than a segment of an isolated rhombic tetramer are ignored, because the orientation of a linear cluster cannot be defined for such a small cluster. Angles of segments are mapped onto their Voronoi regions by color, as shown by the color bar in Fig. B (b).

The same segments are used for the calculation of radial directional correlation, g_θ. The parameters for calculating g_θ is shown in Fig. B (c). For counting the number of end n_end, on the other hand, a skeletonized image before segmentation was used without removing short lines, for evaluating the topological property of a pattern. n_end gives qualitative and relative measure of the connectivity of patches; it is not directly related to the number of bonds between patches.

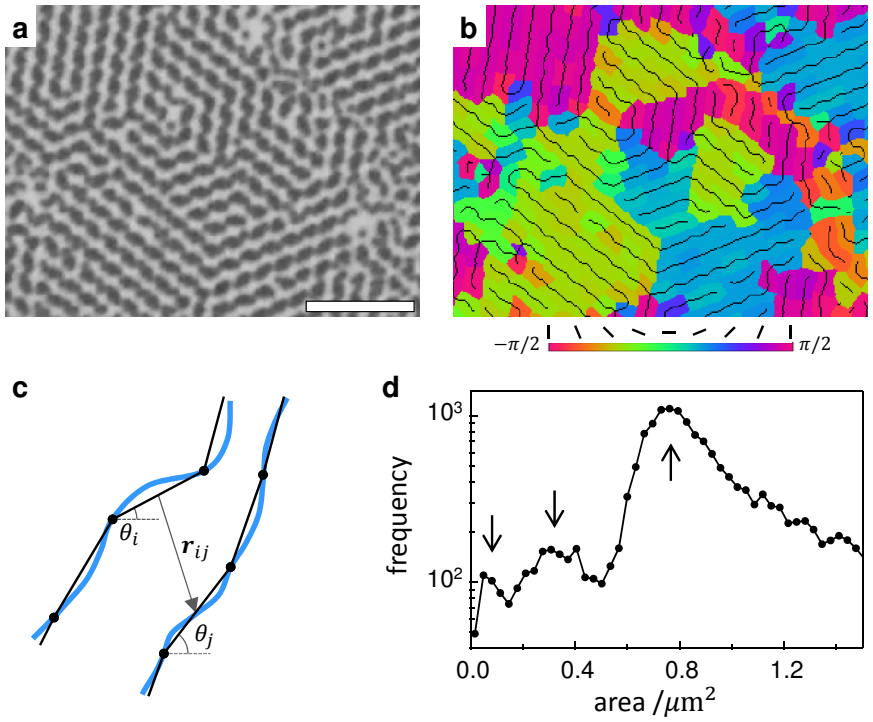

FIG. B Procesures of image processing and analysis with an example. (a): A microscopy image cropped from Fig. 4 (a). (b): A superposition of skeletonized dark regions, i.e. aggregating patches, in (a) onto a color-mapped image obtained from segmented lines. (c): Schematic diagram of segmentation. Thick blue curves are the lines by skeletonization, and black straight lines are the segmented ones. Angles of segment i and j and the vector connecting the centers of the segments are also shown. (d): Histgram of the area of a dark region in the sample of Fig. 7 (c). The arrows indicate the peaks of monomer, dimer and trimer from the left.

Analysis for Fig. 7

In one-patch particles a cluster size (i.e., the number of bonded particles in a cluster) simply equals the number of aggregating patches. The area of a dark region in a microscopy image is approximately proportional to the number of patches, in particular when a linear cluster is long. In small clusters three-dimensional fluctuation of particle orientation affects the apparent area; however, quantized area distribution corresponding to monomer, dimer and trimer is observed in a histogram in Fig. B (d). The horizontal position of the third peak corresponds to the area of decomposed small clusters in Fig. 7 (f). For simplicity we estimate the size of a cluster, $\hat{N}$, by normalizing the area of a dark region, A, with one-third

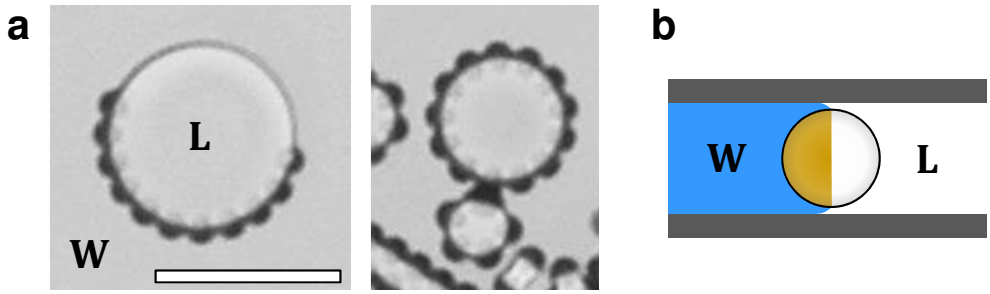

FIG. C Particles attached to the interface of the phase-separated liquids. "L" and "W" denote lutidine- and water-rich phase respectively. (a): Microscopy images for $d = 2.0$ μm, $h_0 = 50$ nm and $\Delta T = 6.0$ K. Scale bar: 10.0 μm. (b): A schematic drawing of the cross-sectional view.

of the area at the peak of trimer, $\bar{A}_3$: $\hat{N} = A/(\bar{A}_3/3)$. Because of the rough estimation, the scale of $\hat{N}$ could deviate a few 10% from the actual number of aggregating patches, N.

RESULTS

Movies

Supplemental movies were recorded during observations of the sample in Fig. 2, 3, 4 and 7. The file name of a movie includes the corresponding figure name like "movie1_fig2b" for Fig. 2 (b). The playing speed in each is accelerated 10 times.

Particles at the interface of phase-separated liquids

Figuer C (a) is an example of hemispherically-patched particles at the interface between water-rich and lutidine-rich phases. A gold patch is in lutidine-rich and bare side is in a water-rich phase. The cell surfaces are hydrophobic, the interface is thus vertical as shown in Fig. C (b).

Other calculated patterns

Some calculated equilibrium patterns by the simulations are shown. Figure D (a) and (b) are the patterns with no patch-substrate attraction, showing the dependence on $\theta_{\rm ap}$ and $e_{\rm b}$,

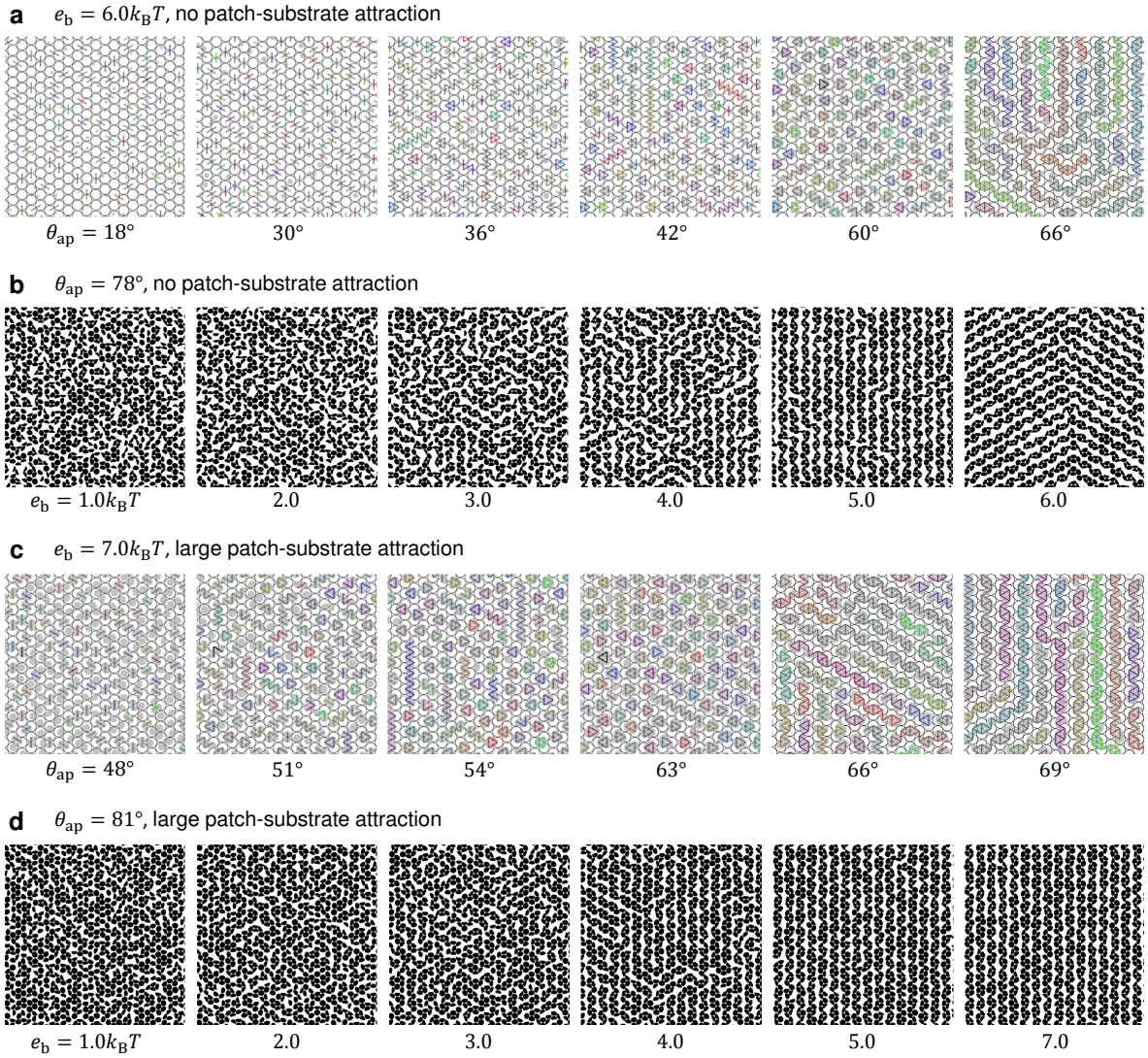

FIG. D Calculated equilibrium patterns by simulation, showing e_b- and θ_{ap}-dependence. Conditions and parameters of each pattern are shown in the figure. Scales are the same for (a) and (c), or (b) and (d).

respectively. Figure D (c) and (d) are the patterns with large patch-substrate attraction.